Catena 147 (2016) 650–662

Contents lists available at ScienceDirect

Catena

journal homepage: www.elsevier.com/locate/catena

Experimental investigation of the effect of vegetation on soil, sediment erosion, and salt transport processes in the Upper Colorado River Basin Mancos Shale formation, Price, Utah, USA

Erik M. Cadaret [a], Sayjro K. Nouwakpo [b,*], Kenneth C. McGwire [a], Mark A. Weltz [c], Robert R. Blank [c]

[a] Desert Research Institute, Division of Earth and Ecosystem Sciences, Reno, Nevada, USA
[b] University of Nevada Reno, Department of Natural Resources and Environmental Science, Reno, Nevada, USA
[c] U.S. Department of Agriculture, Agriculture Research Service, Great Basin Rangelands Research Unit, Reno, Nevada, USA

ARTICLE INFO

Article history:
Received 6 May 2016
Received in revised form 8 August 2016
Accepted 15 August 2016
Available online 24 August 2016

Keywords:
Saline soils
Rangeland Hydrology and Erosion Model
TDS in runoff
Vegetation driven spatial heterogeneity
Dissolution
Price River

ABSTRACT

Because of concerns about salinity in the Colorado River, this study focused on saline and sodic soils associated with the Mancos Shale formation with the objective of investigating mechanisms driving sediment yield and salinity loads and the role of vegetation in altering soil chemistry in the Price-San Rafael River Basin. Rainfall simulations using a Walnut Gulch rainfall simulator were performed at two study sites (Ferron and Price, Utah) across a range of slope angles and rainfall intensities to evaluate the relationship between sediment yield, salinity transport processes, and rainfall-induced changes in soil chemistry. Soil at Ferron had substantially greater salinity than Price as expressed in evaluated sodium absorption ratio, cation exchange capacity in soil, sediment, and total dissolved solids (TDS) in runoff. Principal component analysis and *t*-tests revealed that the two sites have different runoff and soil chemistry ions. Greater concentrations of K^+, NO_3^-, and Cl^- were present in soil-under-vegetation microsites compared to interspace soil areas. Soil soluble phase ions generally increased with depth and underwent vertical fluxes at rates proportional to rainfall intensity. Vegetation appears to have a protective effect on the soils from increasing rainfall intensity. Mat-forming saltbush found at Ferron was related most strongly to soil protection. The dissolution of sediment particles in runoff may be a key component of salinity transport processes on the Mancos Shale. Plot-averaged sediment and TDS had a positive linear relationship. The Rangeland Hydrology and Erosion Model successfully predicted TDS in runoff derived from these upland rangelands in central Utah.

1. Introduction

The Colorado River Basin provides water for millions of people in the western U.S. and Mexico. Before substantial settlement of the west occurred, the salinity load of the Colorado River was estimated to be 600–700 ppm (ppm) in the Lower Colorado River Basin (Blackman et al., 1973). Concerns over increase in river salinity led to the ratification of the Colorado River Basin Salinity Control Act of 1974 to meet treaty obligations with Mexico. Since the Salinity Control Act was enacted, total dissolved solids (TDS) has been reduced by about 1.2 million tons per year (Bureau of Reclamation, 2011). Damages within the United States from dissolved solids in the Colorado River still exceed $380 million per year (Bureau of Reclamation, 2005, 2011). The salinity-control effort has largely focused on reducing dissolved-solids loading from irrigated lands (Bureau of Reclamation, 2011). About 55% of the TDS comes from natural, non-irrigated sources on rangelands (Kenney et al., 2009). This suggests there is significant potential to further reduce dissolved-solids loading to the Colorado River through land- and water-management activities on rangelands.

The most vulnerable rangeland areas in the Upper Colorado River Basin (UCRB) for soil and salt movement are where annual precipitation is between 100 and 400 mm per year which limits soil moisture available to sustain plant growth. With low plant density and minimal plant and ground surface cover, arid and semi-arid areas are prone to both wind and water erosion and transport of salts. Arid and semi-arid regions have low plant density which often results in open and connected bare interspaces where aerodynamic roughness is low and fetch length is sufficient to allow for wind erosion and transport of salts (Okin et al., 2009). In addition, there is insufficient vegetation canopy and ground surface cover to prevent soil or salt movement from raindrop slash, sheet, and rill erosion in the bare connected interspaces

Abbreviations: CEC, cation exchange capacity; ID, immiscible displacement; MASL, meters above sea level; PCA, principal component analysis; RHEM, Rangeland Hydrology Erosion Model; SAR, sodium absorption ratio; TDS, total dissolved solids; VCC, vegetation canopy cover; WGRS, Walnut Gulch rainfall simulator.

* Corresponding author.
E-mail address: snouwakpo@unr.edu (S.K. Nouwakpo).

http://dx.doi.org/10.1016/j.catena.2016.08.024
0341-8162/

(Puigdefabregas, 2005). The relatively low vegetation cover combined with high intensity convective rainfall events makes the UCRB one of the most erosive areas of the United States.

Average sediment yield frequently exceeds 3 tons per hectare per year on the Colorado Plateau (Langbein and Schumm, 1958). As water erosion is exponentially related to rainfall intensity, most of the soil erosion occurs during rare spatially distributed convective storm events. Consequently, rilling and arroyo formation is very pronounced in the Colorado Plateau (West, 1983). Interaction between wind erosion and deposition and water erosion, transport, and deposition is poorly understood. Nevertheless, limited vegetation cover and steep, highly dissected slopes of weathered marine shales in the UCRB make these areas prone to both types of erosion and transport processes. Therefore, total erosion and transport of salts maybe maximized in these arid and semi-arid regions. In Utah, 7–15% of the rangeland areas are classified as being in a severely eroding condition, and 20% of these lands are at risk of accelerated soil erosion (Rasely et al., 1991; Weltz et al., 2014). It is estimated that these areas are responsible for 75–90% of the increasing sediment and salt yields in Utah (Rasely et al., 1991).

The Mancos Shale formation spans a wide area in the UCRB in southeast Utah and has been identified as a major producer of sediment, salinity, and selenium to the Colorado River (Evangelou, 1981; Tuttle et al., 2014a, 2014b). One of the tributaries of the Colorado River, the Price River, contributes <1% of the water, but approximately 3% of the salt load in the Colorado River, with a substantial part of the salt load originating from the Mancos Shale formation (Rao et al., 1984). The majority of the Mancos Shale formation is under the control of the federal government (Bureau of Land Management, National Park Service, and the Bureau of Reclamation). This creates an opportunity to reduce salinity through proactive land and water management practices.

Several studies have investigated salinity transport processes on the Mancos Shale formation and how it relates to soil erosion. Laronne and Shen (1982) conducted a study on the Mancos Shale and determined that several factors of solute pickup are related to sediment erosion processes. These factors include: (1) rate of diffusion from soil minerals to runoff water (2) slope, (3) runoff rate, (4) rill development, and (5) dissolution of transported sediment particles. Ponce (1975) conducted a rainfall simulation study on several geologic members of the Manos Shale formation and found statistically significant linear correlations between TDS and sediment in runoff on individual rainfall plots. Ponce (1975) attributed the variability in the linear correlations to the variability in dissolution rates of suspended sediment particles. Evangelou (1981) showed that when concentrations of Ca^{2+} are high in runoff, the release of ions (primarily Na^{+} and Mg^{2+}) on the Mancos Shale is directly related to and regulated by the exchange complex, represented as the cation exchange capacity (CEC), and the relative cation adsorption affinities of the soil minerals. Therefore, Evangelou (1981) attributes CEC as the mechanism driving a substantial increase in dissolved solids from rangelands on Mancos Shale soils. Currently there are few physically-based models that can predict dissolved solids delivery to the Colorado River system. Nevertheless, if as suggested by Ponce (1975); Evangelou (1981), and Laronne and Shen (1982) that one can relate TDS in runoff to sediment concentration, then there is an opportunity to develop a physically-based framework to predict runoff and TDS from modeled sediment outputs.

A companion study to this study was conducted by Cadaret et al. (2016) to determine if Rangeland Hydrology and Erosion Model (RHEM) (Nearing et al., 2011) can be successfully calibrated for runoff and erosion on the saline and sodic soils of the Mancos Shale formation. Cadaret et al. (2016) investigated how the influence of spatial distribution and total vegetation canopy cover affects RHEM model outputs. The calibrated RHEM model runoff and sediment outputs from Cadaret et al. (2016) is used in this study to relate TDS in runoff to sediment concentration and show that a physically-based framework can be used to predict runoff and TDS from modeled sediment outputs.

This paper analyzes data from rainfall simulation experiments that were performed at two Mancos Shale sites in Utah to measure sediment and dissolved solids loading in response to rainfall intensity and soil physical characteristics. These rainfall simulations were used to determine: (1) soil chemistry differences between sites and spatial differences within each site; (2) the altering effect of vegetation on soil properties and infiltration; (3) what drives salinity transport processes; (4) if a relationship exists between sediment yield and salinity transport processes; and (5) if the relationship can be applied to the RHEM (Nearing et al., 2011) using sediment yield as a proxy to estimate runoff and TDS.

2. Material and methods

2.1. Site description and plot installation

Our study sites are located near Price, Utah in the Price-San Rafael River basin (1.1×10^4 km^2). This sparsely populated area within the Colorado Plateau is characterized by an uplifted, eroded, and deeply dissected tableland with a salt-desert shrubland ecosystem. The average annual air temperature is 8.2 °C (January = −15.6 °C, July = 32.7 °C) and average annual precipitation is 227 mm/yr (November = 13.0 mm, September = 29.2 mm). Runoff is generated from spring snowmelt and short duration, high intensity convectional storms during the summer. The two field sites, named Ferron and Price, were selected because of their location on the Mancos Shale formation, accessibility for field operations, National Environmental Policy Act clearance, and variation in vegetation cover, soil properties, and slope. The Ferron field site (111° 7′ 21″ W, 38° 58′ 23″ N) is at an elevation of 1900 MASL and located 74 km south-southwest Price (Fig. 1). The Price field site (110° 36′ 26″ W, 39° 27′ 47″ N) is at an elevation of 1700 MASL and located 23 km southeast of the city of Price.

The Ferron site is located on the Lower Blue Gate member of the Mancos Shale formation (Doelling and Kuehne, 2013) with a soil mapped as Chipeta-Badland complex (USDA-NRCS, 2013) and Calcic Solonchak according to WRB classification (FAO/ISRIC/ISSS, 2006). Ferron contains poorly developed, light-medium gray soil crusts on steep-grade slopes (11.4%–24.5%) with moderate vegetation cover (17.7%–25.2%). Patches of salt efflorescence on the soil surface are abundant at Ferron. The vegetation at Ferron is solely comprised of the salt-tolerant shrub species *Atriplex corrugata* (i.e. mat saltbush) that is mainly distributed on Mancos Shale derived soils (Blauer et al., 1976). The Price field site is located on the Tununk member of the Mancos Shale formation with a soil mapped as Persayo loam (USDA-NRCS, 2013) and Haplic Calcisol according to WRB classification (FAO/ISRIC/ISSS, 2006). Price contains well developed, light gray soil crusts on shallow-grade slopes (0.6%–10%) with sparse vegetation cover (3.3%–17.8%). The predominant salt-tolerant plant species found at Price are *Ephedra viridis*, *Atriplex gardneri*, and *Achnatherum hymenoides*. Both sites had been recently grazed by cattle and antelope as evidence of hoof impressions were visible across the site.

At each field site, three replicates of four rainfall intensities were performed, for a total of twelve 6×2 m rainfall simulation plots. Rainfall intensities used in this study were derived from 5 min rainfall amounts for the study area from NOAA's Atlas14 database (http://www.nws.noaa.gov/oh/hdsc/index.html). Rainfall intensities were 50.8 mm/h, 88.9 mm/h, 114.3 mm/h, and 139.7 mm/h respectively for the 2-, 10-, 25-, and 50-year storms. One of the plots at Price (#12) was excluded in this paper because the rainfall simulation duration was unusually long, resulting in significantly greater cumulative runoff. Each plot was aligned along the natural contour of the land, allowing flow concentration toward the center of each plot to existing rills that would carry water down-gradient. At the top and side borders of each plot, steel strips (2×0.2 m) were installed to contain runoff within the measurement area. A flume equipped with pressure transducers was installed at the bottom of the plot to monitor runoff discharge. The position of the

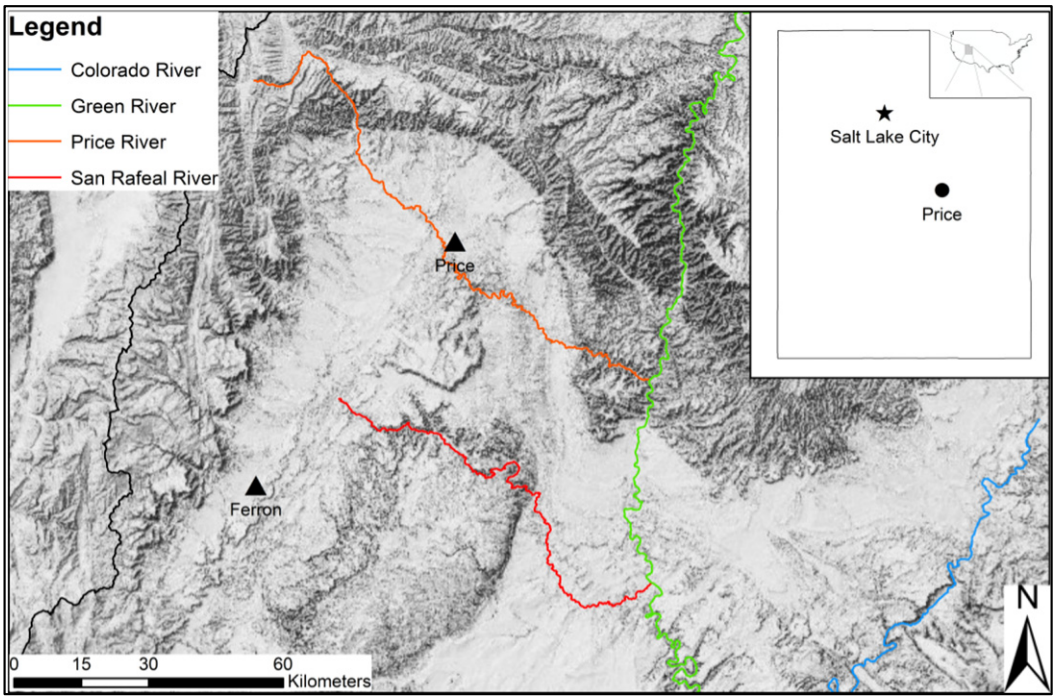

Fig. 1. Map of the field sites relative to rivers in the Upper Colorado River Basin. Reproduced from Cadaret et al., 2016.

plot was shifted within a couple meters up or downslope of the selected location so that the bottom edge was at a point that is as level as possible. The edge of the collection pan for the flume has a 90-degree bend on the upslope side with an edge that extends downwards approximately 3 cm. This edge was gently pressed on the soil surface to identify its position and then removed. Hand tools are used to create a clean, sharp cut in the soil surface along that line, being as careful as possible to minimize disturbance of the soil crust on the upslope side. The collection pan was then carefully installed as flush as possible with the bottom of the existing rill channel. Flexible metal sheets were placed at the upslope corners of the pan and secured to the pan and side rails with spring-loaded clamps in order to ensure that all flow is captured. A clear plexiglass sheet covered the collection pan to ensure that overspray from the simulator was not counted in the measurement of flow. The plexiglass cover is supported by the edge of the collection pan and V-shaped steel supports that were placed on the pan, well back from the upslope edge. At the bottom of the collection pan is a flume with a 4% supercritical slope that empties into a drainage trench where samples are collected. A computer-controlled Walnut Gulch rainfall simulator (WGRS) (Paige et al., 2004) was used for rainfall simulations that completely and evenly covered the plot (Fig. 2). Water used to perform rainfall simulations was transported from the Bureau of Land Management office in Price, Utah.

2.2. Field measurements

Runoff was collected during each simulation using two different collection containers. Runoff water chemistry samples were collected

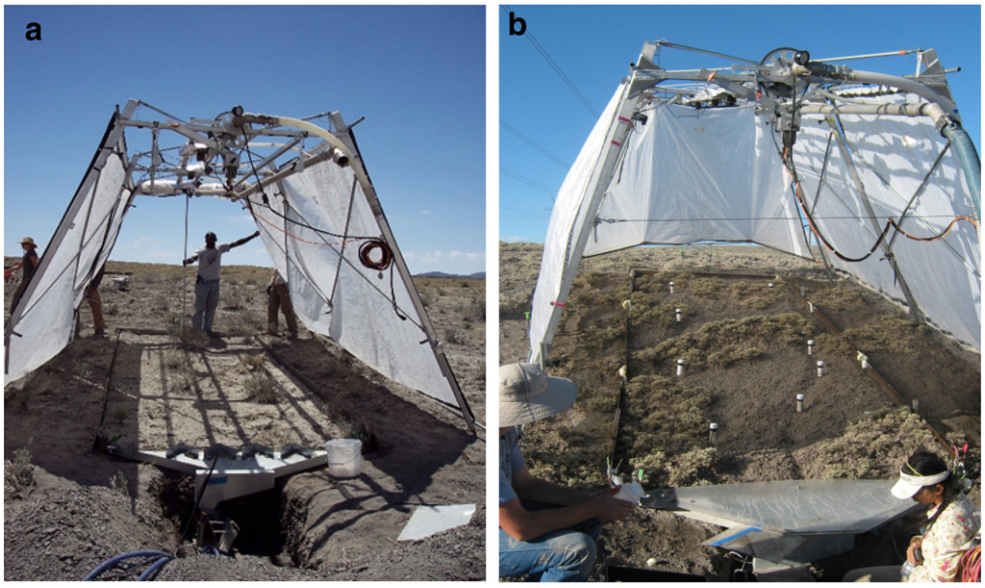

Fig. 2. Walnut Gulch rainfall simulator operating at Price (a) and Ferron (b), Utah.

using 50 mL centrifuge tubes and sediment samples were collected using 1 L Nalgene bottles, neither of which was pretreated. Runoff was collected following initiation of flow. On the first field expedition to the Price site, ten rainfall simulations were completed. On that trip, sampling was performed every thirty seconds for the first nine minutes and then every minute thereafter over the fifteen-minute simulation duration following initiation of runoff. On the second field expedition for two additional plots at Price and twelve plots at Ferron, runoff was collected every thirty seconds for the first three minutes and then every three minutes until discharge measured by the flume flow gauge reached equilibrium (i.e. 10 min without change in measured discharge). The sampling protocol was changed because examination of hydrographs from the first field expedition indicated the simulations were not run long enough for the discharge to consistently reach steady-state and there were insufficient resources to maintain the original sampling rate for a longer duration. Before each rainfall simulation, the applied water was sampled from the water tank in one 50 mL centrifuge tube to measure simulated rain water quality. The runoff water chemistry samples were covered with para-film around the cap to reduce the chance of leakage, placed in large plastic bags, and stored inside coolers with dry ice in order to reduce subsequent bacterial chemical reactions. The sediment samples were stored without refrigeration in plastic crates. A total of 473 runoff water chemistry samples were collected (including 24 applied rainfall water chemistry samples): 275 from Price and 198 from Ferron. A total of 263 sediment samples were collected: 133 from Price and 130 from Ferron.

Slopes for each plot were measured using a Nikon NPR 352 total station (Nikon-Trimble Co. Ltd., Tokyo, Japan). Soil cores were collected pre- and post-rainfall. The pre-rainfall soils were collected on the control plots using a trowel due to the lack of soil cohesion as a result of the low soil moisture content. Post-rainfall soils samples were collected using a 25 cm long AMS split soil core with a 5 cm inside diameter. Pre- and post-rainfall soil samples were collected at three locations under the vegetation canopy and at three bare soil (interspace) locations. At each soil sample location, soils were separated into a surface sample and two subsurface samples (0–1 cm; 1–5 cm; 5–10 cm) (Fig. 3). Finally, soil samples from the vegetation and interspace microsites within each plot were mixed to make one composite soil sample for each microsite (i.e. vegetated versus interspace). The soil samples were stored in plastic bags and placed in a cooler with refrigeration. A total of 192 soil samples were collected: 96 from Price and 96 from Ferron.

2.3. Laboratory analysis

Each runoff water chemistry sample was centrifuged at 2000 rpm for three minutes to settle any sediment that may be present. Soluble cations of Ca^{2+} and Mg^{2+} in runoff were quantified using atomic absorption spectroscopy, and K^+ and Na^+ in runoff were quantified by atomic emission spectroscopy using a Perkin Elmer atomic absorption (AA) spectrometer (PerkinElmeer, Inc., Waltham, Massachusetts, USA). Ammonium (NH_4^+) was measured using a Lachat Quickchem Flow Injection Analysis + instrument (Hach Company, Loveland, Colorado, USA). Soluble anions (NO_2^-, NO_3^-, SO_4^{2-}, Cl^-) in runoff were measured using a Dionex ion chromatograph (IC) (Dionex Co., Sunnyvale, California, USA) with a AS18-4 μ column. Price and Ferron runoff water chemistry samples required dilution to be within a linear range on both the AA and IC instruments. Ortho-phosphorous (Ortho-P) was below detection limit for nearly all samples. Runoff pH and electro-conductivity (EC) were measured in the lab using an Oakton 510 series pH Meter and VWR Scientific model 2052 EC Meter, respectively.

For soil samples, soluble-phase cations and anions were extracted by immiscible displacement (ID) (Mubarak and Olsen, 1977). Solution-phase anions (NO_2^-, NO_3^-, SO_4^{2-}, Cl^-) were measured using the Dionex IC with a AS11-HC column. Some samples that were very high in SO_4^{2-} and Cl^- required dilution to be within the linear range of the IC. Solution-phase Ca^{2+} and Mg^{2+} were quantified using atomic absorption spectroscopy and K^+ and Na^+ using atomic emission spectroscopy with the AA spectrometer. Some samples very high in Na^+ required dilution. Soil mineral N (NO_2^-, NO_3^-, NH_4^+) was extracted using 1.5 M KCl (Bundy and Meisinger, 1994) and quantified on the Lachat system. Cation exchange capacity (CEC) was measured according to methods of Bower et al. (1952). The solution-phase ion solution produced by ID was measured to quantify pH and EC using an Oakton 510 series pH Meter and VWR Scientific model 2052 EC Meter, respectively.

2.4. Data analysis

2.4.1. Differences between sites

Differences in chemistry of runoff water and soils between sites and between vegetated and interspace areas at each site were visualized using principal components analysis (PCA). PCA is a statistical method for transforming a diverse set of measurements into a number of uncorrelated linear combinations, called eigenvectors, that represent rotations of the axes of measurement within the multidimensional space of the measured variables. The resulting eigenvectors indicate which patterns of correlation between the original measurements explain the majority of variation in the entire dataset. The first eigenvector, expressed as a set of weights for each of the original variables, explains the majority of variance in the entire dataset. The eigenvector of each subsequent PCA axis is uncorrelated with the preceding ones and explains the majority of the residual variance that is not captured by its predecessors. The greater the value of the eigenvector weight, the more important that variable is in explaining that component of variation in the entire dataset. The signs of the eigenvector weights indicate which variables are operating in unison (same sign) or opposition (opposite signs). Thus, in a dataset where all measurements increased or decreased together, the first PCA eigenvector would typically have all positive weights while the second PCA axis would use positive and negative signs to indicate the most pervasive pattern of contrasts between these correlated variables. The score of each data sample for each PCA axis can be calculated by multiplying the eigenvector weight for each variable against the original data value and summing those weighted

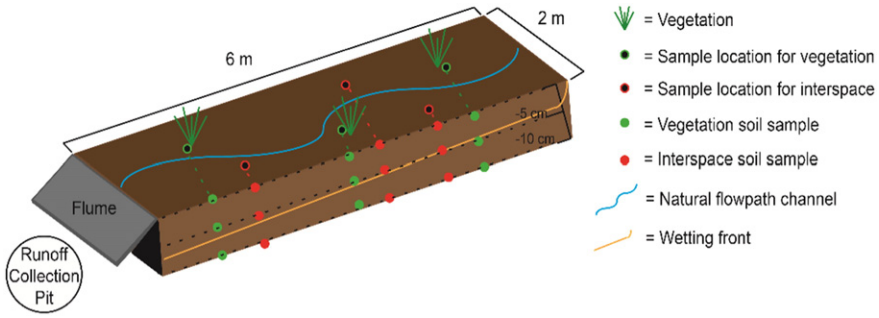

Fig. 3. Conceptual drawing of the plot setup and sampling locations for runoff and soil.

values. This transformation can be used to show how PCA-derived patterns of variability are related to membership in different experimental subsets (e.g. location, vegetation type, slope class). In this study, the PCA used correlation rather than covariance matrices to ensure that results were not affected by the varying ranges of input variables. To compliment the PCA analysis, two-sample *t*-test analysis was used to identify which ions were significantly different. All soil immiscible displacement (ID) data was used in this analysis.

The average slope, runoff total dissolved solids (TDS), sediment, soil sodium absorption ratio (SAR), and soil cation exchange capacity (CEC) were calculated for each plot. TDS was calculated as the sum of all ion concentrations in mg/L. Soil SAR and CEC was calculated from soil ID data.

2.4.2. Transient soil ion fluxes

Stepwise multiple linear regression analysis was performed on the sums of soluble-phase cations and anions (meq/L) for all plots collated by rainfall intensity for each site to assess the effect of depth (cm), rainfall intensity (mm/h), and microsite on solute mobility in the soil profile. The regression model was set up with an α to enter = 0.1 and an α to remove = 0.11. This alpha value was used instead of a more common 0.05 because of the relatively low number of soil samples ($n < 100$). R^2_{Pred}, a leave one out validation statistic, was used to evaluate if the regression model provides valid predictions. If the difference between R^2 and R^2_{Pred} is >0.1, this indicates the model over-fits outliers in the data and is not reliable (Myers et al., 2012). All soil ID data were used in this analysis.

2.4.3. Salinity transport processes

Stepwise multiple linear regression analysis was done for TDS (mg/L) in runoff to identify which variables are most strongly related to salinity transport. The variables that were tested included several proposed from Laronne and Shen (1982) (applied water TDS (mg/L), slope (%), discharge (L/s), sediment (kg/L)), from Ponce (1975) (sediment yield (kg/L)), and from Evangelou (1981) (surface crust soil CEC (cmol+/kg), ratio of runoff Ca^{2+} concentration to TDS concentration), and others we thought may contribute to salinity transport (surface crust soil salinity, surface crust soil SAR, rainfall intensity, and vegetation canopy cover (VCC; %)). The regressions used plot-averaged values for each variable. The TDS regression model was set up with an α to enter = 0.05 and an α to remove = 0.05. We chose a more restrictive alpha because by using the plot-averaged data ($n = 23$) instead of the raw data ($n > 100$) as there was a substantial reduction in variability and improvement in model performance. Again, R^2_{Pred} was used to validate the regression model. Location (Ferron, Price) was included as a categorical predictor in the model, so that site differences in each factor would be accounted for.

2.4.4. Sediment as a proxy for salinity

Linear regression analysis was done for sediment yield (kg/L) versus TDS in the runoff (mg/L) in order to investigate if sediment concentration can be used as a proxy for TDS concentration when using the RHEM model. Average TDS in runoff and sediment were calculated for each respective plot. Sediment and water chemistry were not sampled simultaneously and were collected at differing rates, so it was appropriate to use a type II "errors-in-variables" regression model that does not assume regression error is entirely attributable to the dependent variable. Use of ordinary least squares (OLS) regression in these cases results in an attenuation of the slope coefficient that provides biased predictions (overestimation of low values, underestimation of high values). A number of type II regression methods exist (e.g. Deming regression, orthogonal regression), and here we use reduced major axis (RMA; type II) regression. Reduced major axis regression makes no assumptions about dependence of the regressed relationship (Friedman et al., 2013) and minimizes the sum of triangular areas between data points and the best fit line (Carr, 2012).

Estimates of cumulative runoff and sediment yield for each 12 m^2 plot from the RHEM model (Cadaret et al., 2016) were converted into L and kg/L, respectively. The RMA linear regression model for predicting TDS in runoff from sediment (from Section 2.4.3) was used with RHEM-simulated plot-averaged sediment yield (kg/L) to predict associated TDS in runoff (mg/L). The result of this analysis was assessed using the ratio of the root mean squared error to observed range ($RMSE/O_{RA}$) for all TDS data and by determining if a 1:1 relationship falls within the 95% confidence interval of the RMA regression line.

The ratio of the root mean squared error to observed range ($RMSE/O_{RA}$) was calculated using the following equation:

$$\frac{RMSE}{O_{RA}} = \frac{\sqrt{\frac{\sum_{i=1}^{n}(O_i - P_i)^2}{n}}}{O_{max} - O_{min}} \quad (1)$$

where n is the total number of plots, P_i is the simulated value by the model for the corresponding ith plot, Oi is the observed ith plot to be evaluated, O_{max} is the maximum observed value and O_{min} is the minimum observed value for all TDS data.

Table 1
Descriptive statistics for slope, TDS, sediment concentration, and soil SAR and CEC for both sites.

Site	Sample	Mean	SE[a]	Units
Price	Slope	0.063	0.008	%
	TDS	216	19.8	mg/L
	Sediment	0.030	0.002	kg/L
	Soil SAR	0.146	0.017	N/A
	Soil CEC	9.123	0.080	cmol+/kg
Ferron	Slope	0.190	0.009	%
	TDS	630	32.1	mg/L
	Sediment	0.105	0.005	kg/L
	Soil SAR	35.2	2.6	N/A
	Soil CEC	12.231	0.117	cmol+/kg

[a] SE = standard error of the mean.

3. Results

3.1. Differences between sites

Table 1 shows the mean values for slope, TDS, sediment yield, soil SAR, and soil CEC. For each, there is a substantial difference between the two field sites.

Principal component analysis of runoff water chemistry illustrates that the first principal component (PC1) explains 45% of the variance

Table 2
PCA Eigenvectors for each ion from both field sites for runoff and soil chemistry.

PCA	PC	Ca^{2+} meq/L	Mg^{2+} meq/L	Na^{+} meq/L	K^{+} meq/L	NH_4^{+} meq/L	NO_3^{-} meq/L	SO_4^{2-} meq/L	Cl^{-} meq/L
Runoff	1	−0.351	0.108	−0.464	−0.447	−0.199	0.283	0.408	0.406
	2	−0.464	−0.482	0.134	0.069	0.594	0.028	0.388	−0.163
Soil	1	0.442	0.334	−0.477	0.33	−0.243	0.082	0.412	0.348
	2	−0.087	−0.323	−0.146	−0.516	0.112	0.593	0.163	0.457

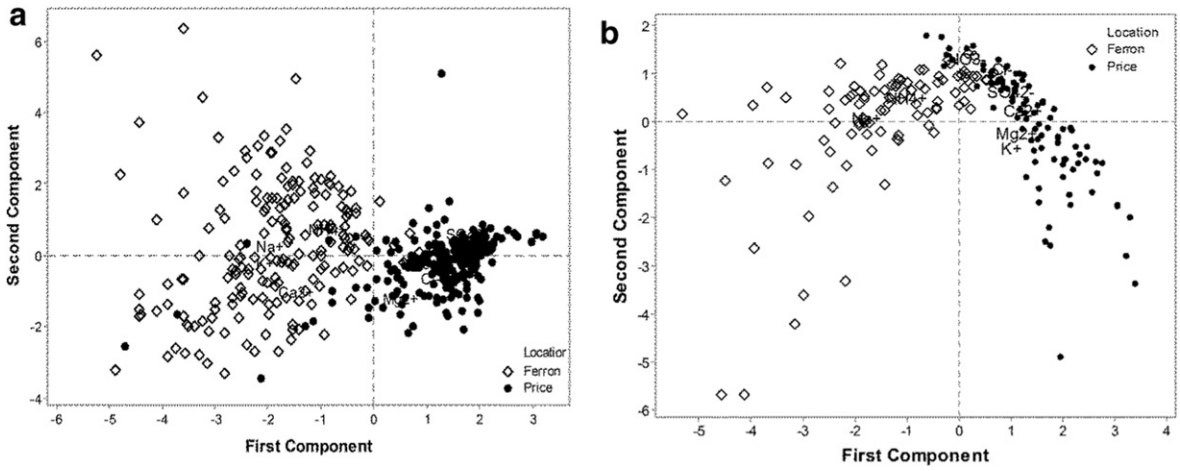

Fig. 4. Score plot for the first and second principal components for (a) runoff chemistry and (b) soil chemistry classified by site.

in measurements and the second principal component (PC2) explains an additional 20%. The PC1 eigenvector for runoff chemistry (Table 2) indicates that the most pervasive pattern of variation across the entire dataset is a negative correlation of Na^+ and K^+ versus SO_4^{2-} and Cl^-. A plot of PCA scores (Fig. 4a) shows that the variability described by PC1 is associated with differences between the two field sites, though a few cases of overlap between the clusters indicate that some plots from Price had similar runoff chemistry as the Ferron site. PCA results for soil chemistry (control and post-rainfall samples) show that the PC1 explains 40% of the variance and the PC2 explains an additional 20%. For the soil chemistry data, the primary pattern of variability (PC1) is expressed as a negative correlation of Ca^{2+} and SO_4^{2-} versus Na^+ and NH_4^+ (Table 2). The soil PCA score plot shows an even stronger differentiation between the two sites in the soils data (Fig. 4b) than in the runoff data (Fig. 4a). For PC2 of the soil chemistry data, the two sites diverge from one another in a linear pattern indicating there may be a similar phenomenon that contributes to variation in soil chemistry at both sites once the site differences have been accounted for.

t-Test results indicate that all ions in runoff were significantly different between sites (n_1 (Ferron) = 267, n_2 (Price) = 186, $p < 0.001$) and Ferron runoff had substantially greater average ion concentrations (Table 3). Mg^{2+} in runoff for both sites and Cl^- for Price had negative concentrations because there was a greater concentration of the ion in the water applied during rainfall simulations than there was dissolved in runoff. Except nitrate, all ions in soil were significantly different between sites (n_1 (Ferron) = 96, n_2 (Price) = 96, $p < 0.003$). Price soils

Table 3
t-Test results from both field sites for runoff and soil chemistry.

t-Test	Ion	Location	*n*	Mean (meq/L)	SD	SE	*p*	*t*	diff.[a]	df	95% CI
Runoff	Ca^{2+}	Ferron	187	4.080	2.590	0.190	<0.001	8.15	1.846	331	(1.4, 2.291)
		Price	267	2.240	2.010	0.120					
	Mg^{2+}	Ferron	187	−1.970	0.641	0.047	<0.001	−4.25	−0.214	241	(−0.314, −0.115)
		Price	267	−0.953	0.298	0.018					
	Na^+	Ferron	187	3.620	1.720	0.130	<0.001	28.46	3.609	187	(3.359, 3.86)
		Price	267	0.013	0.160	0.010					
	K^+	Ferron	187	0.264	0.072	0.005	<0.001	20.82	0.142	391	(0.128, 0.155)
		Price	267	0.123	0.701	0.004					
	NH_4^+	Ferron	187	0.023	0.025	0.002	<0.001	7.03	0.014	240	(0.01, 0.018)
		Price	267	0.010	0.012	0.000					
	NO_3^-	Ferron	187	0.016	0.021	0.002	<0.001	8.27	0.013	209	(0.01, 0.016)
		Price	267	0.003	0.006	0.000					
	SO_4^{2-}	Ferron	187	9.730	6.280	0.460	<0.001	12.19	6.202	266	(5.2, 7.204)
		Price	267	3.520	3.530	0.220					
	Cl^-	Ferron	187	0.303	0.133	0.001	<0.001	28.06	0.310	285	(0.288, 0.332)
		Price	267	−0.006	0.084	0.005					
Soil	Ca^{2+}	Ferron	96	9.880	3.700	0.380	<0.001	−14.72	−9.417	173	(−10.679, −8.154)
		Price	96	19.300	5.060	0.520					
	Mg^{2+}	Ferron	96	1.475	0.696	0.071	<0.001	−7.87	−2.050	110	(−2.567, −1.534)
		Price	96	3.530	2.460	0.250					
	Na^+	Ferron	96	79.200	58.700	6.000	<0.001	13.14	78.710	95	(66.82, 90.60)
		Price	96	0.478	0.533	0.054					
	K^+	Ferron	96	0.496	0.203	0.210	<0.001	−8.53	−0.570	114	(−0.702, −0.438)
		Price	96	1.066	0.622	0.063					
	NH_4^+	Ferron	96	0.015	0.027	0.003	0.003	3.00	0.009	132	(0.003, 0.015)
		Price	96	0.006	0.012	0.002					
	NO_3^-	Ferron	96	0.421	0.474	0.048	0.21	1.26	0.081	186	(−0.046, 0.208)
		Price	96	0.340	0.417	0.043					
	SO_4^{2-}	Ferron	96	79.400	55.300	5.600	<0.001	9.11	51.820	98	(40.53, 63.1)
		Price	96	27.540	7.260	0.740					
	Cl^-	Ferron	96	2.610	3.500	0.360	<0.001	6.37	2.285	96	(1.573, 2.996)
		Price	96	0.321	2.840	0.029					

[a] diff. = difference in meq/L between the means.

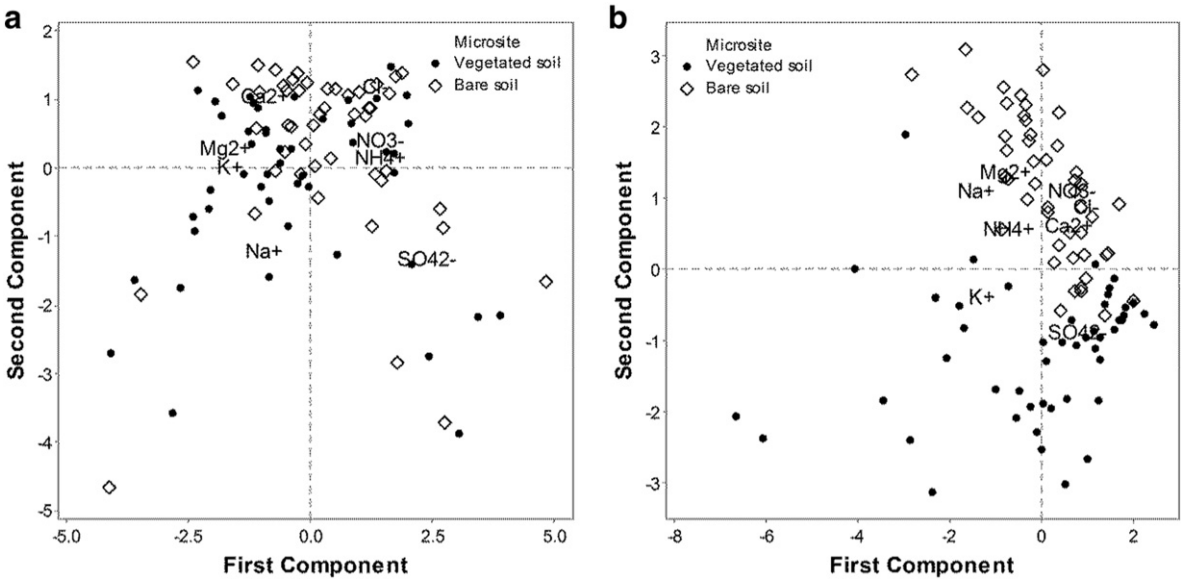

Fig. 5. Score plot for the first and second principal components for (a) Price soil chemistry and (b) Ferron soil chemistry classified by microsite.

had greater concentrations of Ca^{2+}, Mg^{2+}, and K^+, whereas Ferron soils had greater concentrations of Na^+, NH_4^+, SO_4^{2-}, and Cl^-. In addition, the ratio of Ca^{2+} to Mg^{2+} is greater at Ferron than at Price.

The PCA for soil chemistry at Price alone showed that PC1 explains more than a third of the variation (37%) in measurements and PC2 explains an additional 22% of the variance. The score plot shows substantial overlap between canopy and interspace microsites in both PCA axes (Fig. 5a). The greater similarity in variance explained by PC1 and PC2 and the overlap in Fig. 5a indicates a relatively weak distinction between the soil chemistry of microsites at Price. *t*-Test results for Price soils indicate that K^+, NO_3^-, and Cl^- are significantly different between microsites (n_1 (Vegetation) = 48, n_2 (Interspace) = 48, $p < 0.008$). Soil under vegetation has greater concentrations of these ions than interspace soils (Table 4). A lack of microsite differentiation in Fig. 5a

Table 4
T-Test results from both field sites for vegetated and interspace soil areas.

t-Test	Ion	Location	*n*	Mean (meq/L)	SD	SE	*p*	*t*	diff.[a]	df	95% CI
Price	Ca^{2+}	Vegetation	48	19.420	5.330	0.770	0.81	0.24	0.25	93	(−1.81, 2.31)
		Interspace	48	19.170	4.840	0.700					
	Mg^{2+}	Vegetation	48	3.370	2.040	0.290	0.527	−0.63	−0.319	85	(−1.32, 0.681)
		Interspace	48	3.690	2.830	0.410					
	Na^+	Vegetation	48	0.533	0.496	0.072	0.311	1.02	0.111	92	(−0.105, 0.327)
		Interspace	48	0.423	0.568	0.082					
	K^+	Vegetation	48	1.233	0.678	0.098	0.008	2.72	0.335	87	(0.09, 0.579)
		Interspace	48	0.898	0.515	0.074					
	NH_4^+	Vegetation	48	0.007	0.012	0.002	0.773	0.29	0.001	93	(−0.004, 0.006)
		Interspace	48	0.006	0.012	0.002					
	NO_3^-	Vegetation	48	0.482	0.532	0.077	0.001	3.52	0.283	56	(0.122, 0.444)
		Interspace	48	0.198	0.166	0.024					
	SO_4^{2-}	Vegetation	48	27.460	7.590	1.100	0.913	−0.11	−0.16	93	(−3.12, 2.8)
		Interspace	48	27.620	7.000	1.000					
	Cl^-	Vegetation	48	0.406	0.274	0.039	0.003	3.03	0.169	93	(0.058, 0.279)
		Interspace	48	0.237	0.272	0.039					
Ferron	Ca^{2+}	Vegetation	48	183.600	97.200	14.000	0.057	−1.94	−28.9	58	(−58.7, 0.9)
		Interspace	48	212.500	34.900	5.000					
	Mg^{2+}	Vegetation	48	1.043	0.495	0.071	<0.001	−7.75	−0.865	90	(−1.087, −0.644)
		Interspace	48	1.908	0.594	0.086					
	Na^+	Vegetation	48	55.500	60.100	8.700	<0.001	−4.30	−47.3	88	(−69.2, −25.4)
		Interspace	48	102.800	47.000	6.800					
	K^+	Vegetation	48	0.598	0.229	0.033	<0.001	5.70	0.204	62	(0.133, 276)
		Interspace	48	0.394	0.096	0.014					
	NH_4^+	Vegetation	48	0.013	0.016	0.002	0.372	0.90	0.005	66	(−0.016, 0.006)
		Interspace	48	0.178	0.035	0.005					
	NO_3^-	Vegetation	48	0.615	0.578	0.083	<0.001	4.37	0.387	58	(0.21, 0.565)
		Interspace	48	0.228	0.208	0.030					
	SO_4^{2-}	Vegetation	48	54.900	54.100	7.800	<0.001	−4.82	−48.9	90	(−69.1, −28.7)
		Interspace	48	103.800	44.900	6.500					
	Cl^-	Vegetation	48	4.100	4.280	0.620	<0.001	4.62	2.996	56	(1.697, 4.295)
		Interspace	48	1.110	1.360	0.200					

[a] diff. = difference in meq/L between the means.

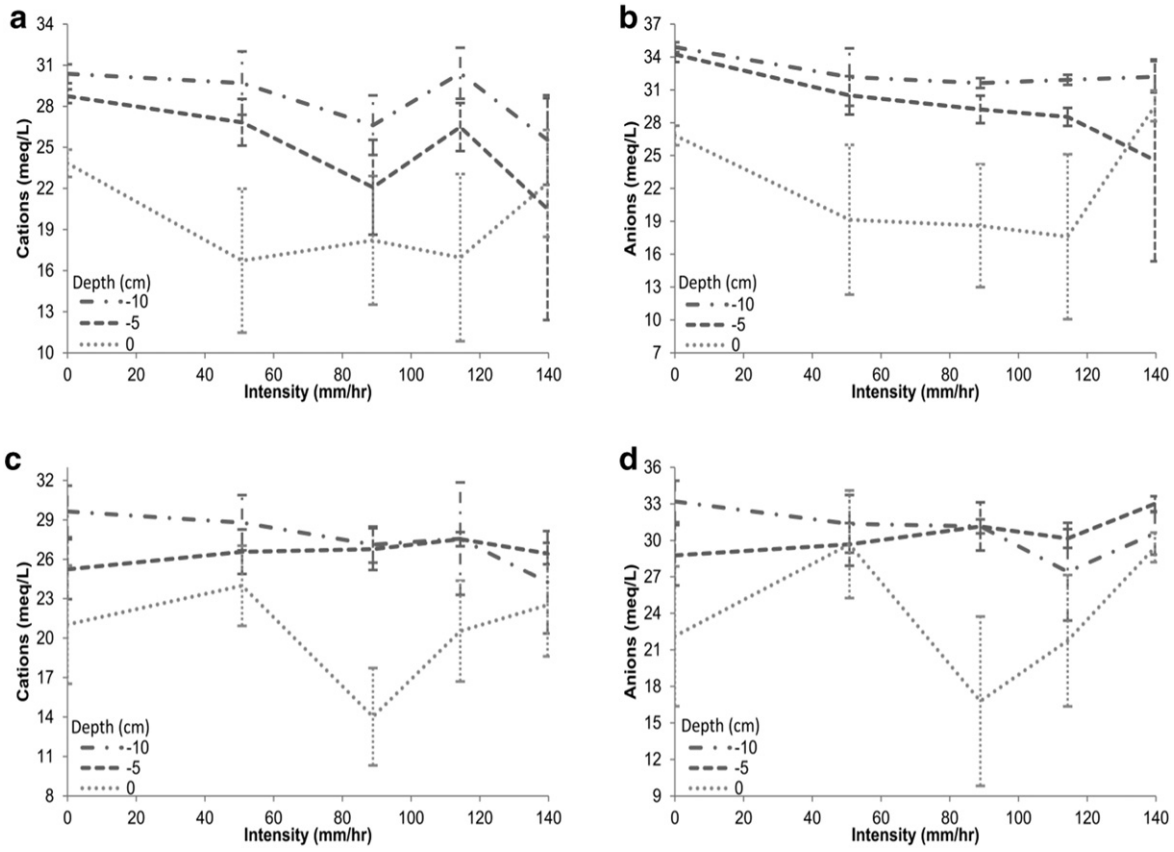

Fig. 6. Transient soil ion flux for Price (a) cations and (b) anions in soil under vegetation, and (c) cations and (d) anions in interspace soil.

indicates that these differences are a relatively weak effect compared to the overall sample variance.

PC1 of Ferron soil chemistry between microsites explains 33% of the variation in measurements, and PC2 explains an additional 29%. While there is substantial overlap between microsites in PC1 (Fig. 5b), there is a noticeable difference in soil chemistry between microsites in PC2. Thus, while the majority of variation in microsite soil measurements (PC1) is not associated with vegetated versus interspace areas, the similarity in variance explained by PC2 and the clustering of Fig. 5b show that there is a well-defined difference in microsite chemistry at Ferron. *t*-Tests for Ferron soils indicate that Mg^{2+}, Na^{+}, K^{+}, NO_3^-, SO_4^{2-}, and Cl^- are significantly different between microsites (n_1 (Vegetation) = 48, n_2 (Interspace) = 48, $p < 0.001$) and Ca^{2+} is on the cusp of being significantly different ($p = 0.057$) (Table 5). Ca^{2+}, Mg^{2+}, Na^{+}, and SO_4^{2-} have greater concentrations in interspace soils whereas K^{+}, NO_3^-, and Cl^- have greater concentrations in soils under vegetation.

3.2. Transient soil ion fluxes

Figs. 6 and 7 show the transient ion fluxes within the soil profile in response to rainfall intensity at Price and Ferron soils under vegetation (a–b) and interspace soils (c–d). The results show that only the models of soil cations ($n = 30$, $R^2 = 0.647$, $p < 0.001$) and anions ($n = 30$, $R^2 = 0.483$, $p < 0.001$) at Price provided valid predictions ($|R^2_{Pred} - R^2| < 0.1$). The residual and normal probability plots and the Anderson-Darling normality test ($p > 0.05$) showed no significant departure from normality. Soil depth explained the majority of the variability in concentration of soil cations ($R^2 = 0.593$, $p < 0.001$) and anions ($R^2 = 0.483$, $p < 0.001$) and the effect was most pronounced for cations. Rainfall intensity explained a negligible portion of the variability ($R^2 = 0.054$, $p = 0.052$) for soil cations. Even though the models of soil cations and anions at Ferron were not strongly supported by R^2_{Pred} or the residual and normal probability plots, Fig. 7 shows similar trends to those that are evident at Price (Fig. 6).

Fig. 6 shows that cation and anion concentrations generally increase with depth at Price for both microsites and this effect is most pronounced for cations. Fig. 7c–d shows soil cations and anions decreased with depth at Ferron only for interspace soils. This finding suggests that at both Price and Ferron, surface layers were depleted of ions at interspace soils compared to deeper soil. The same trend was also observed for Price in soil under vegetation. From field operations, it was observed in several soil pits dug at Price where runoff is collected that deep in the soil profile (>10 cm), salt crystals may accumulate in fractured shale void spaces. Price also had well developed soil crusts whereas Ferron had patches of salt efflorescence. Both may indicate the surface layers were enriched in certain ions, but overall had an inconsequential effect on total ion concentration.

Price and Ferron both generally show that rainfall intensity has a decreasing effect for cations and anions at both microsites (Figs. 6 and 7) that affected both surface and deeper layers of the soil profile. The effect is most pronounced at Price for soils under vegetation (Fig. 6a–b) and Ferron for interspace soils (Fig. 7c–d). This finding suggests that at both Price and Ferron, soil ions generally decrease with increasing rainfall intensity. However, there was a significant increase in surface soil anions between the 114.3 mm/h and 139.7 mm/h for Price vegetated and interspace soils. The same trend, even though not significant, is also present for the cations and shows a decrease in cations in the deeper layers. There is also a significant decrease in surface soil cations and anions at Price interspace soils between 50.8 mm/h and 88.9 mm/h.

Ferron (Fig. 7) shows a more pronounced difference in cation and anion concentrations between microsites than Price (Fig. 6) which is

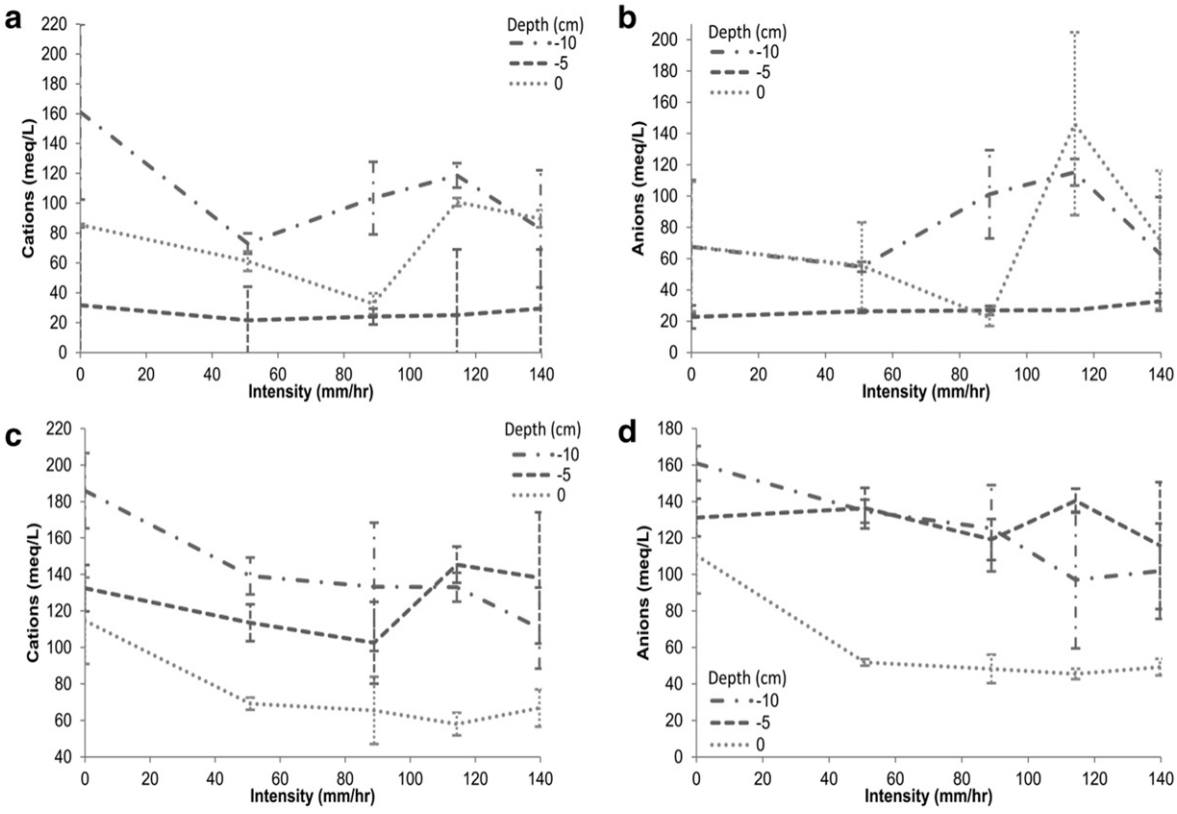

Fig. 7. Transient soil ion flux for Ferron (a) cations and (b) anions in soil under vegetation, and (c) cations and (d) anions in interspace soil.

consistent with the results from Section 3.1 (Fig. 5; Table 4). We also see the effects of depth and rainfall intensity at Ferron is more pronounced. Ions in soil under vegetation at Ferron (Fig. 7c–d) did not consistently decrease with depth or rainfall intensity. This suggests that the vegetation canopy cover at Ferron has a protective effect on the soil under the canopy.

3.3. Salinity transport processes

Stepwise multiple linear regressions identified which variables are most strongly related to salinity transport, including those proposed by Laronne and Shen (1982), Ponce (1975), and Evangelou (1981). Sediment was the only variable that explained a significant proportion of the variance in runoff salinity ($n = 23$, $R^2 = 0.821$, $p < 0.001$), with $R^2_{pred} = 0.778$ indicating that the model is not over-fitting outliers. Regression results are summarized in Table 5. The residuals (Fig. 8a) appear to have a random distribution with no outliers greater than three standard deviations from the mean. The QQ-norm plot (Fig. 8b) does not reveal any problematic departure from normality and neither does the Anderson-Darling test (AD = 0.445, $p = 0.260$).

3.4. Sediment as a proxy for TDS in runoff

RMA linear regression was used to determine whether predicted sediment from RHEM could be used as a proxy to estimate TDS in runoff. Using the plot-averaged data of observed sediment and TDS in runoff, a strong, positive relationship exists between sediment and TDS (Fig. 9). Average sediment significantly predicted TDS in runoff ($n = 23$, $R^2 = 0.819$, $p < 0.001$). Using this relationship to estimate plot-averaged TDS in runoff from the sediment output predicted by RHEM (Cadaret et al., 2016), Fig. 10 shows a strong linear relationship also exists between observed TDS concentrations and sediment predicted by RHEM ($n = 23$, $R^2 = 0.73$, $p < 0.001$). A 1:1 relationship falls within the 95% confidence interval for the slope of the RMA regression line. The RMSE

Table 5
Stepwise multiple linear regression results for runoff salinity concentration.

Coefficients						
Term	Coefficient	SE	95% CI	*t*	*p*	VIF
Constant	80.1	47.3	(−18.1, 178.2)	1.69	0.105	
Sediment concentration	4864	484	(3860, 5867)	10.05	<0.001	1.00
ANOVA						
Model	df	SS	Contribution	MS	*F*	*p*
Regression	1	1,902,582	82.1%	1,902,582	101.07	<0.001
Error	22	414,134	17.9%	18,824		
Total	23	2,316,717	100.0%			

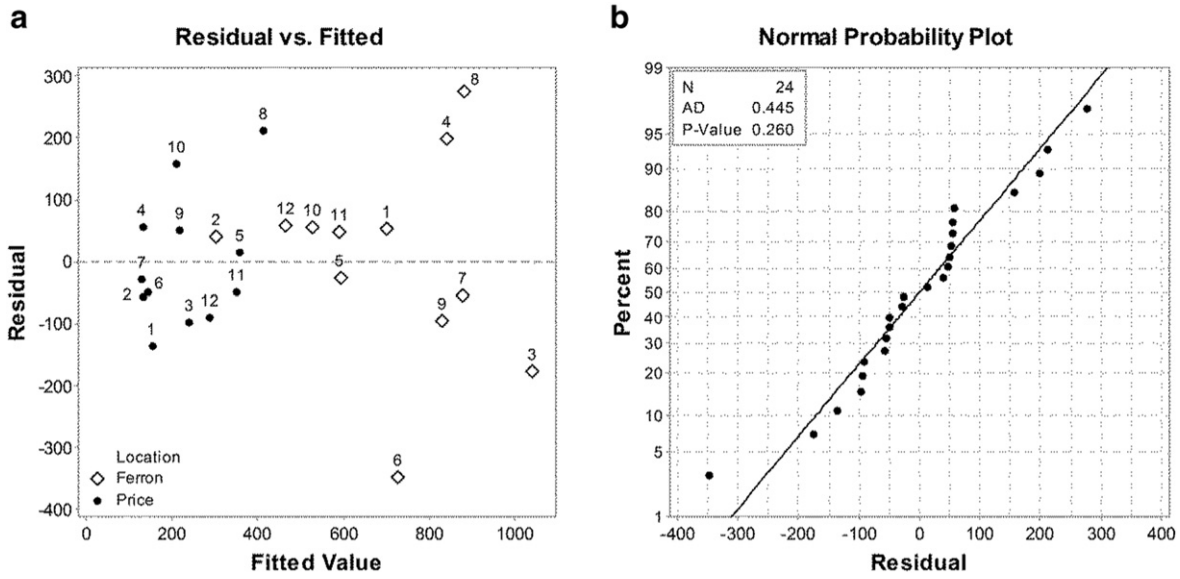

Fig. 8. Residual and normal probability plots for multiple regression on plot averaged TDS in runoff. (a) Residual plot of regression. Point data labels = plot number. (b) Normal probability plot of regression.

between observed and estimated TDS concentration is 170.2 mg/L and the ratio of RMSE to O_{RA} is 0.149 indicating that the linear regression model provides valid predictions with a low error relative to the observed range of values.

4. Discussion

This study found significant differences in soil and runoff chemistry between sites on different geologic members of the Mancos Shale formation. Ferron had steep slopes that produced substantially more TDS and sediment in runoff. Ferron soil also had a higher SAR and CEC (Table 1) than soil at Price. The PCA and *t*-test results indicate that the soil chemistry and runoff is significantly different between sites for almost every ion measured (Fig. 4; Table 2). The differences in runoff and soil chemistry between sites may be related to the difference in each sites respective depositional environment during the late Cretaceous. Differences in parent material in arid climates typically drive differences in soil development which influences the type of vegetation that may grow on these soils.

This study also showed that Price and Ferron had significantly different soil chemistry between microsites (Table 4) suggesting vegetation has an effect on altering soil chemistry. *t*-Tests indicate that for both sites, K^+, NO_3^-, and Cl^- were in significantly greater concentrations in soils under vegetation, but the magnitudes of difference were more pronounced at Ferron (Table 3). Zucca et al. (2011) conducted a study in Morocco looking at the effects of *Atriplex nummularia* growth on soil chemical properties and found significantly greater concentrations of K^+ and SAR under the canopy at sampling locations with good to moderate vegetation development. A study by Sharma and Tongway (1973)

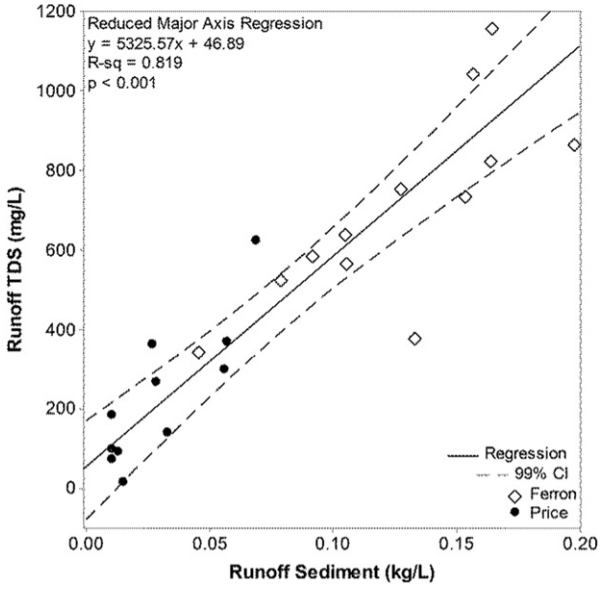

Fig. 9. Regression of plot-averaged sediment vs. TDS in runoff.

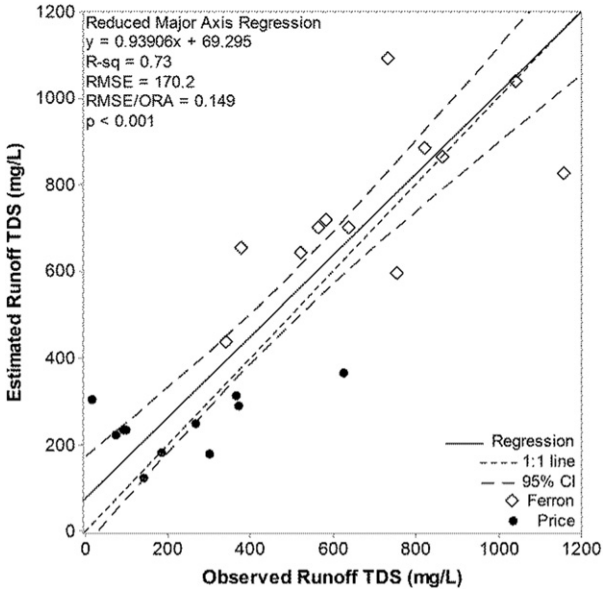

Fig. 10. Regression of the plot-averaged observed TDS in runoff vs. estimated TDS in runoff relative to the 1:1 line.

Fig. 11. Images showing differences vegetation structure between Price (left) and Ferron (right), Utah (reproduced from Cadaret et al., 2016).

investigated the effects of *Atriplex nummularia* and *Atriplex vesicaria* on the spatial variability of ions in the soil profile found greater concentrations of Cl^- underneath both plants in Australia. Sharma and Tongway also found that soils underneath *A. nummularia* had greater soil salinity compared to *A. vesicaria* likely because *A. nummularia* has a greater amount of litter fall per unit area under the canopy resulting in more available salt to be leeched from the litter. Sharma (1973) reported that an increase in salinity is strongly correlated to chlorides of various cations. Charley and West (1975) investigated plant-induced soil chemical patterns in shrub-dominated areas of Utah. They found greater concentrations of total nitrogen under the canopy of *Atriplex* vegetation. Our findings and prior work collectively suggest that biogeochemical cycling by plants (Blank et al., 1992) led to increased K^+, NO_3^-, and Cl^- concentrations under the canopy and seems to be dependent on the amount and type of vegetation present. *Atriplex* plants generally reduce and stabilize soil salinity (Salem et al., 2010; Blauer et al., 1976) beneath the canopy and in turn may reduce TDS in runoff. Fig. 11 shows pictures illustrating the difference in vegetation structure between Price and Ferron.

In the field, we observed that the mat-forming saltbush (*Atriplex corrugata*) at Ferron provides more protective canopy cover than the vegetation at Price which has less contact with the soil surface and a more open canopy. This added protection within vegetated areas at Ferron likely contributed to the difference in soil chemistry between microsites. From field observations, we noted that the soil supporting vegetation at Ferron was significantly higher in elevation (i.e. coppice dunes) compared to the surrounding area while elevation differences within vegetated and interspace surfaces were less pronounced. The greater elevation difference between vegetated areas and interspace at Ferron was likely facilitated by the higher degree of rilling due to the steep slopes at the site. As a result, runoff tends to concentrate in the interspace and is deflected around the vegetation (Urgeghe et al., 2010; Puigdefabregas, 2005; Howes and Abrahams, 2003). At Ferron, this vegetation driven spatial heterogeneity results in concentrated flow contained within the interspaces. This leads to reduced ion mobility and transport in the soil profile under vegetation (Fig. 7a–b). At Price, runoff flows through interspaces and sparsely vegetated areas alike resulted in a more uniform vertical mobility of ions across the plot (Fig. 6).

Our results show that there is a depletion of cations and anions with increasing rainfall intensity and an increase in ions with depth for Price and Ferron interspace soils and Price soils under vegetation (Figs. 6 and 7c–d). Sharma and Tongway (1973) also reported that salinity generally increased with increasing depth. Sharma (1973) also found the same trend for cations and SAR. However, Zucca et al. (2011) instead observed a decrease in soil cations with depth. The general decrease in ions with rainfall intensity is consistent with a vertical flux of ions, the orientation of which depends on the relative dominance of advection and diffusion processes. An increase in rainfall intensity is correlated with an increase in runoff depth, greater infiltration rates (calculated by subtracting discharge from rainfall for each plot), and potentially a deeper wetting front. Average infiltration rate across study sites increased from 20.7 mm/h for low intensity rainfall events (<100 mm/h) to 24 mm/h for high intensity rainfall events (>100 mm/h). While the wetting front depth was not specifically measured in this study, one would expect the increase in wetting front depth with runoff depth combined with the low soil matric potential of the initially dry soil to result in an increase in wetting front depth with intensity. This would also be expected to be much larger than the increase in the eroded layer at the soil surface (the average thickness of soil lost is estimated at 1.7 mm assuming a bulk density of 1.3 g/cm^3 at both sites). The decrease in soil ions with increasing intensity can therefore be explained by an increase in downward advective fluxes of water and dissolved elements with rainfall intensity. An increase in runoff depth would also be associated with an increase in the concentration gradient from the ion-rich soil solution relative to the runoff. An upward diffusion of ions from soil to runoff and subsequent transport off-site would then decrease solute concentrations within the soil profile. The relative importance of these advective and diffusive processes cannot be evaluated in this study but merit further experimental investigation. Nevertheless, soil ions did not increase with depth for soils under vegetation at Ferron (Fig. 7a–b). The middle soil layer at −5 cm depth was the most depleted compared to the surface and −10 cm depth soil. The enrichment of soil ions at the surface may be a result of increased leeching of ions from the plant and litter at the surface. The depletion in the mid layer (−5 cm) may be a result of biogeochemical cycling and the adventitious roots structure of the mat-saltbush.

Several mechanisms have been proposed to explain the complex relationship between soil erosion, sediment yield, and salinity transport processes (Ponce, 1975; Evangelou, 1981; Laronne and Shen, 1982). Ponce (1975) studied soil erosion and salinity transport processes on the Mancos Shale formation near our study area in the Price River watershed. Ponce conducted rainfall simulations with variable rainfall intensity (25–75 mm/h) over time (60 and 100 min). Ponce found statistically significant correlations between suspended sediment and TDS in runoff for several plots located on the undivided Mancos (R^2 = 0.28–0.81) and the Upper Blue Gate Member (R^2 = 0.00–0.46) of the Mancos Shale formation. Ponce attributed the variability in the linear correlations to be representative of the variability in dissolution rates of suspended sediment particles. The Ferron site (Lower Blue Gate member) produced greater runoff EC than Price (Tununk member), a trend Ponce also found.

Laronne and Shen (1982) direct runoff study on the Mancos Shale formation investigated several mechanisms to explain the variability in TDS in runoff and to also verify the findings by Ponce (1975).

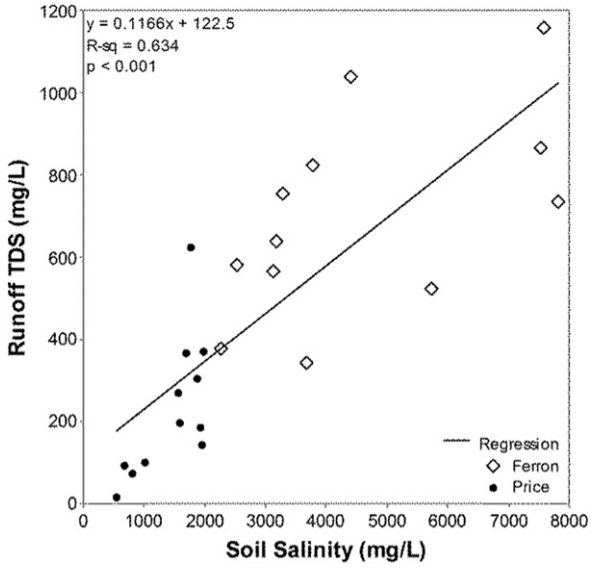

Fig. 12. Regression of the plot-averaged soil salinity vs. TDS in runoff.

Evangelou (1981) conducted a chemical and mineralogical study to investigate the diffuse source of salts from the Mancos Shale formation and concluded that CEC is the mechanism that drives a substantial increase in salinity loading on Mancos Shale soils. Our findings (Figs. 8 and 9; Table 4) show that only one variable out of the many proposed by Ponce, Laronne and Shen, and Evangelou was significant. We found a strong correlation between plot-averaged sediment concentration and TDS in runoff across both sites. This suggests the primary process related to salinity transport is the detachment and dissolution of sediment particles in runoff. This confirms the findings by Ponce (1975) and Laronne and Shen (1982). However, this gives rise to an important question: how much dissolution of the sediment particles occurred?

Ponce (1975) performed 1:1 soil: water extracts to investigate the relationship between soil salinity and TDS in runoff and found a high linear correlation between soil EC and runoff EC of the soil:water extracts. Our study supports those findings (Fig. 12).

The ratio of TDS in runoff to soil salinity varied between 3 and 35%, suggesting that 65–97% of the transported salts in runoff were still attached to suspended sediment particles. This result suggests that the proportion of salt dissolved in runoff may be controlled primarily by mechanical action (e.g., detachment of sediment particles by raindrop impact and frictional forces during transport) and physiochemical disintegration of aggregates due to the dispersing effect of some cations on clay minerals (feedback mechanism). The latter may be related to soil CEC (Evangelou, 1981), but needs to be confirmed with further research.

Despite the significant differences observed, RHEM-simulated sediment from Cadaret et al. (2016) was applied to the regression model (Fig. 9) and a strong, significant relationship between the observed TDS and RHEM-estimated TDS (Fig. 10) was found with relatively low error. This indicates that sediment can be used as a proxy to estimate TDS in RHEM using our linear regression model. It also indicates soil erosion, sediment yield, and salinity transport processes are highly related. This suggests that reducing runoff and soil erosion will reduce in salt mobility and salinity transport processes.

At this time, more research is needed to understand the kinetics of salt dissolution in runoff during hillslope erosion and transport processes of the Mancos Shale formation. This information will be useful in the design of management and mitigation strategies. One possible course of action to reduce TDS in runoff is to promote deposition of sediment along the runoff pathway (Nouwakpo et al., 2016). Cadaret et al. (2016) found the amount and specific spatial distribution of VCC is related to soil erosion and transport processes. A strategic placement of vegetation to enhance deposition may be a possible course of action to reduce sediment yield and TDS in runoff. Improving our understanding of mechanisms that control deposition and salt dissolution kinetics will help in the proper scaling of knowledge learned at the plot scale in this study. Our findings and that of Cadaret et al., 2016 are relevant to the plot scale and may not linearly upscale to broader spatial domains. Further research on sediment and hydrological connectivity in these arid and semi-arid environments is also needed for adequate transfer of information up and down spatial scales.

5. Conclusion

In this study, we found that the runoff chemistry and the soil chemistry between the two sites had significantly different ion concentrations that may be a result of the differences in soil development of the parent material. Soils underneath vegetation were found to have greater concentrations of K^+, NO_3^-, and Cl^-. This is likely a result of geochemical cycling by plants as reported in previous studies. Soluble phase ions generally decreased with increasing rainfall intensity and increased with increasing depth indicating greater vertical ion fluxes with an increase in the amount of water that infiltrated into the soil. The relationship was not consistent across both sites. At the Ferron site, the dense network of vegetated islands on soil pillars resulted in less movement of ions. This suggests that a means of controlling salinity transport is through enhancing vegetation density and the spatial distribution of vegetation.

This study showed soil erosion (i.e. sediment concentration and sediment yield) to be linearly related to salinity transport processes ($R^2 = 0.82$) by the detachment and dissolution of sediment particles. The ratio of TDS to soil salinity indicated that 65–97% of the transported salts in runoff were still attached to suspended sediment particles. This suggests that dissolution rates may be primarily controlled by mechanical action and physiochemical disintegration of aggregates, but further research is needed to better understand this process. The relationship was used to estimate TDS concentration using simulated sediment concentration from the calibrated RHEM model (Cadaret et al., 2016) and had relatively low error ($R^2 = 0.73$) and a good fit to the 1:1 line. This linear relationship between sediment yield and salinity transport processes can be applied to the RHEM model to estimate TDS entering the Upper Colorado River Basin River network from soils derived from the Mancos Shale formation. Further research is needed to see if these relationships are universal for other saline and sodic soils (e.g. Eagle Valley Evaporite soils) before methods to quantify TDS from all rangelands within the UCRB can be estimated with confidence.

Acknowledgements

This study was funded by the US DOI Bureau of Reclamation, Bureau of Land Management, USDA Agricultural Research Service (Cooperative Agreement 59-5370-3-001), in collaboration with the Desert Research Institute and the University of Nevada, Reno of the Nevada System of Higher Education. USDA is an equal opportunity provider and employer. Mention of a proprietary product does not constitute a guarantee or warranty of the product by USDA or the authors, and it does not imply its approval to the exclusion of the other products that also may be suitable.

References

Blackman Jr., W.C., Rouse, J.V., Schillinger, G.R., Shafer Jr., W.H., 1973. Mineral pollution in the Colorado River basin. J. Water Pollut. Control Fed. 45 (7), 1517–1557.

Blank, R.R., Palmquist, D.E., Young, J.A., 1992. Plant-soil relationships of greasewood, Torrey saltbush, and *Allenrolfea* that occur on coarse-textured mounds on playas. General Technical Report INT-US Dep. of Agric., For. Serv. Intermountain Research Station (USA)

Blauer, A.C., Plummer, A.P., McArthur, E.D., Stevens, R., Giunta, B.C., 1976. Characteristics and hybridization of important intermountain shrubs. II. Chenopod family. USDA For Serv Res Pap INT US Dep. Agric. Intermt. For Range Exp. Stn.

Bower, C.A., Reitemeier, R.F., Fireman, M., 1952. Exchangeable cation analysis of saline and alkali soils. Soil Sci. 73, 251–261.
Bundy, L.G., Meisinger, J.J., 1994. Nitrogen availability indices. In: Weaver, R.W., Angle, S., Bottomley, P., Bezdicek, D., Smith, S., Tabatabai, A., Wollum, A. (Eds.), Methods of Soil Analysis. Part 2. Microbiological and Biochemical Properties. Soil Sci. Soc. of Am. J., Madison, WI, pp. 951–984.
Cadaret, E.M., McGwire, K.C., Nouwakpo, S.K., Weltz, M.A., Saito, L., 2016. Vegetation canopy cover effects on sediment erosion processes in the Upper Colorado River Basin Mancos Shale formation, Price, Utah, USA. Catena 147, 334–344.
Carr, J., 2012. Orthogonal regression: a teaching perspective. Int. J. Math. Educ. Sci. Technol. 43 (1), 134-10. http://dx.doi.org/10.1080/0020739X.2011.573876.
Charley, J.L., West, N.E., 1975. Plant-induced soil chemical patterns in some shrub-dominated semi-desert ecosystems of Utah. J. Ecol. 63 (3), 945–963. http://dx.doi.org/10.2307/2258613.
Doelling, H.H., Kuehne, P.A., 2013. Geologic map of the Short Canyon quadrangle, Emery County, Utah. Utah Geological Survey, Map 255DM, scale 1:24,000.
Evangelou, V.P., 1981. Chemical and Mineralogical Composition and Behavior of the Mancos Shale as a Diffuse Source of Salts in the Upper Colorado River Basin. University of California, Davis.
FAO/ISRIC/ISSS, 2006. World reference base for soil resources 2006. A framework for international classification, correlation and communication. World Soil Resources Reports 103. FAO, Roma.
Friedman, J., Bohonak, A.J., Levine, R.A., 2013. When are two pieces better than one: fitting and testing OLS and RMA regressions. Environmetrics 24 (5), 306–316. http://dx.doi.org/10.1002/env.2213.
Howes, D.A., Abrahams, A.D., 2003. Modeling runoff and runon in a desert shrubland ecosystem, Jornada Basin, New Mexico. Geomorphology 53, 45–73.
Kenney, T.A., Gerner, S.J., Buto, S.G., Spangler, L.E., 2009. Spatially referenced statistical assessment of dissolved-solids load sources and transport in streams of the Upper Colorado River Basin. U.S. Geological Survey Scientific Investigations Report 2009–5007 50 p.
Langbein, W.B., Schumm, S.A., 1958. Yield of sediment in relation to mean annual precipitation. Amer. Geo. Union Trans. 39, 1076–1084.
Laronne, J.B., Shen, H.W., 1982. The effect of erosion on solute pickup from Mancos Shale hillslopes, Colorado, USA. J. Hydrol. 59 (1), 189–207.
Mubarak, A., Olsen, R.A., 1977. A laboratory technique for appraising in situ salinity of soil. Soil Sci. Soc. Am. J. 41, 1018–1020.
Myers, R.H., Montgomery, D.C., Vining, G.G., Robinson, T.J., 2012. Generalized Linear Models: With Applications in Engineering and the Sciences. 791. John Wiley & Sons.
Nearing, M.A., Wei, H., Stone, J.J., Pierson, F.B., Spaeth, K.E., Weltz, M.A., Flanagan, D.C., Hernandez, M., 2011. A rangeland hydrology and erosion model. ASABE 54 (3), 901–908.
Nouwakpo, S.K., Weltz, M., Williams, C., Al-Hamdan, O., Green, C., Accepted, 2016. Insight into sediment transport processes on saline rangeland hillslopes using three-dimensional soil microtopography changes. Earth Surf. Process. Landf.
Okin, G.S., Parsons, A.J., Wainwright, J., Herrik, J.E., Bestelmeyer, B.T., Peters, D.C., Fredrickson, E.L., 2009. Do changes in connectivity explain desertification? Bioscience 59, 237–244.
Paige, G.B., Stone, J.J., Smith, J.R., Kennedy, J.R., 2004. The Walnut Gulch rainfall simulator: a computer-controlled variable intensity rainfall simulator. American Soc. of Agric. Eng. 20 (1), 25–31.
Ponce II, S.L., 1975. Examination of a non-point source loading function for the Mancos Shale wildlands of the Price River Basin, Utah. All Graduate Theses and Dissertations. Paper 3498.
Puigdefabregas, J., 2005. The role of vegetation patterns in structuring runoff and sediment fluxes in drylands. Earth Surf. Process. Landf. 30, 133–147. http://dx.doi.org/10.1002/esp.1181.
Rao, B.K., Bowles, D.S., Wagenet, R.J., 1984. Salt efflorescence in Price River basin. J. Environ. Eng. 110 (2), 457–471.
Rasely, R.C., Roberts, T.C., Pyper, G.P., 1991. Upper Colorado River Basin Rangeland Salinity Control Project: Watershed Resource Condition Evaluation Phase II Procedure. Colorado River Basin Salinity Forum.
Salem, H.B., Norman, H.C., Nefzaoui, A., Mayberry, D.E., Pearce, K.L., Revell, D.K., 2010. Potential use of oldman saltbush (*Atriplex nummularia* Lindl.) in sheep and goat feeding. Small Rumin. Res. 91 (1), 13–28.
Sharma, M.L., 1973. Soil physical and physico-chemical variability induced by *Atriplex nummularia*. J. Range Manag. 26, 426–430.
Sharma, M.L., Tongway, D.J., 1973. Plant induced soil salinity patterns in two Saltbush (*Atriplex* spp.) communities. J. Range Manag. 26, 121–125.
Tuttle, M.L.W., Fahy, J.W., Elliott, J.G., Grauch, R.I., Stillings, L.L., 2014a. Contaminants from cretaceous black shale: I. Natural weathering processes controlling contaminant cycling in Mancos shale, southwestern United States, with emphasis on salinity and selenium. Appl. Geochem. 46, 57–71. http://dx.doi.org/10.1016/j.apgeochem.2013.12.010.
Tuttle, M.L.W., Fahy, J.W., Elliott, J.G., Grauch, R.I., Stillings, L.L., 2014b. Contaminants from cretaceous black shale: II. Effect of geology, weathering, climate, and land use on salinity and selenium cycling, Mancos shale landscapes, southwestern United States. Appl. Geochem. 46, 72–84. http://dx.doi.org/10.1016/j.apgeochem.2013.12.011.
United States Bureau of Reclamation, 2005. Quality of Water Colorado River Basin Progress Report No. 22. U.S. Department of Interior accessed April 1, 2016 at http://www.usbr.gov/uc/progact/salinity/pdfs/PR22.pdf.
United States Bureau of Reclamation, 2011. Quality of Water – Colorado River Basin Progress Report No. 23. U.S. Department of Interior 76 pages, accessed April 1, 2016 at http://www.usbr.gov/uc/progact/salinity/pdfs/PR23final.pdf.
United States Department of Agriculture – Natural Resources Conservation Service, 2013s. Web soil survey national cooperative soil survey. https://soilseries.sc.egov.usda.gov/OSD_Docs/P/PERSAYO.html and https://soilseries.sc.egov.usda.gov/OSD_Docs/C/CHIPETA.html.
Urgeghe, A.M., Breshears, D.D., Martens, S.N., Beeson, P.C., 2010. Redistribution of runoff among vegetation patch types: on ecohydrological optimality of herbaceous capture of run-on. Rangel. Ecol. Manag. 63, 497–504.
Weltz, M., Nouwakpo, S.K., Rossi, C., Jolley, L., Frasier, G., 2014. Salinity mobilization and transport from rangelands: assessment, recommendations, and knowledge gaps. General Technical Report. 1 Reno, Nevada. 61.
West, N.E., 1983. Great Basin-Colorado Plateau sagebrush semi-desert. Temperate Deserts and Semi-deserts. Elsevier Publishing Company, Amsterdam, The Netherlands, pp. 331–349.
Zucca, C., Julitta, F., Previtali, F., 2011. Land restoration by fodder shrubs in a semi-arid agro-pastoral area of Morocco. Effects on soils. Catena 87 (3), 306–312.